

Elemental analysis with a full-field X-ray fluorescence microscope and a CCD photon-counting system

Takuji Ohigashi,^a Norio Watanabe,^{a*} Hiroki Yokosuka,^a Tatsuya Aota,^a Hidekazu Takano,^a Akihisa Takeuchi^b and Sadao Aoki^a

^aInstitute of Applied Physics, University of Tsukuba, 1-1-1 Tennoudai, Tsukuba, Ibaraki 305-8573, Japan, and

^bSPRING-8, Mikazuki, Hyogo 679-5198, Japan.

E-mail: watanabe@bk.tsukuba.ac.jp

The first result is presented of an X-ray fluorescence microscope with a Wolter mirror in combination with a CCD camera used as an energy-resolved two-dimensional detector in photon-counting mode. Two-dimensional elemental maps of metallic wires, such as Fe, Co, Ni and Cu, and inclusions of a synthesized diamond could be obtained with an energy resolution of 350 eV.

Keywords: CCD cameras; photon counting; X-ray fluorescence; X-ray microscopes; Wolter mirrors.

1. Introduction

Direct X-ray detection charge-coupled devices (CCDs) are now widely used as imaging X-ray spectrometers in the photon-counting mode, especially in astronomy (Strüder, 2000). When the incidence X-ray flux is sufficiently low, electron clouds generated in the absorption layer by individual photons do not overlap one another so that the number of electrons in the cloud corresponds to the energy of the X-ray photon. If a photon-counting CCD camera is used as a detector of a full-field X-ray fluorescence microscope, it is possible to perform two-dimensional elemental analysis without changing the energies of the excitation X-rays. This idea has been proposed since the early stage of the development of the CCD camera (Stern *et al.*, 1983). Tsunemi, Wada *et al.* (1991) demonstrated an energy-resolved X-ray fluorescence image by using a photon-counting CCD camera and a pinhole camera. However, because of the lack of an efficient objective lens, no experimental results have been reported about a combination of a full-field X-ray fluorescence microscope with a focusing lens and a photon-counting CCD camera.

Recent developments of X-ray optical elements make it possible to fabricate an X-ray full-field microscope above several keV. Typical objective lenses are a zone plate (Kagoshima *et al.*, 2000), a compound refractive lens (Lengeler *et al.*, 2001) and a Wolter mirror (Aoki *et al.*, 1998). Among these optical elements, a Wolter mirror is the most suitable for an objective of a full-field X-ray fluorescence microscope because it has no chromatic aberration and it can be used for simultaneous imaging of polychromatic X-rays as in X-ray fluorescence. Furthermore, its collecting power is one or two orders of magnitude larger than the other optical elements.

We have been developing a full-field X-ray fluorescence microscope with a Wolter mirror objective (Takeuchi *et al.*, 2000). Using the *K*-edge subtraction method with this microscope, two-dimensional and three-dimensional elemental analysis have been successfully demonstrated (Yamamoto, Watanabe, Takeuchi, Takano, Aota, Fukuda & Aoki, 2000; Watanabe *et al.*, 2001). In this report, we show experimental results of two-dimensional elemental analysis by using a CCD photon-counting system.

2. Optical system

The optical system of the microscope is shown in Fig. 1. An X-ray full-field fluorescence microscope was constructed at beamline 39XU of SPRING-8. This beamline has an in-vacuum-type linear undulator, a rotated-inclined Si(111) double-crystal monochromator and a Pt-coated plane mirror (SPRING-8, 1998). Monochromatic X-rays in the energy range 6–10 keV were used for excitation. The photon energy of the fundamental harmonic was tuned in this energy range. The X-rays of higher harmonics were suppressed by the Pt-coated plane mirror with a grazing angle of 7 mrad. The optical axis of the microscope was set normal to the excitation X-rays to reduce scattering X-rays from the specimen (Takeuchi *et al.*, 2000). The fluorescent X-rays were enlarged by the Wolter mirror and focused on the CCD camera (C4880 system, Hamamatsu Photonics; CCD: TC-215, Texas Instruments). The pixel size was 12 $\mu\text{m} \times 12 \mu\text{m}$ and the total number of pixels was 1000 \times 1018. The CCD was cooled down to 243 K. The average readout noise was 15 electrons r.m.s. The readout frame rate was 4 s per frame. A shutter was not used to prevent detection of X-rays during the readout. The excitation area of the specimen was restricted to be about 1 mm² by changing the slit width in front of the specimen. The energy profile of the fluorescent X-rays could be measured by a solid-state detector (SSD) at the image plane.

The specification of the Wolter mirror is shown in Fig. 2. The mirror surface is coated with Pt to enhance the reflectivity of X-rays. The grazing-incidence angle is 7 mrad and X-rays up to 12 keV can be focused. Its numerical aperture is 0.0258 and the field of view is calculated to be about 200 μm , assuming that the spatial resolution is better than 1 μm (Aoki, 1998). However, the spatial resolution of an

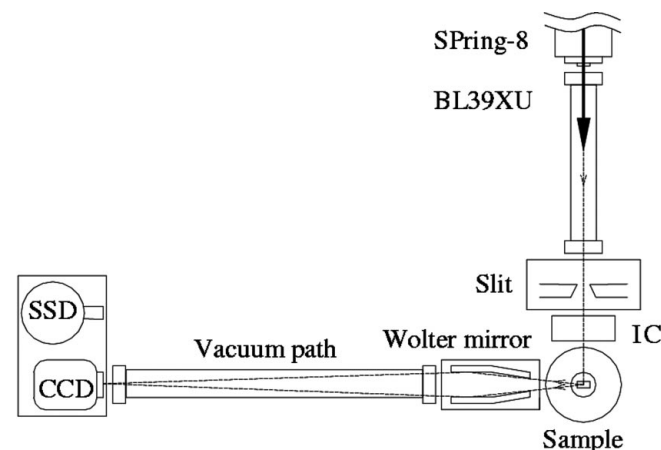


Figure 1
Schematic diagram of the full-field X-ray fluorescence microscope.

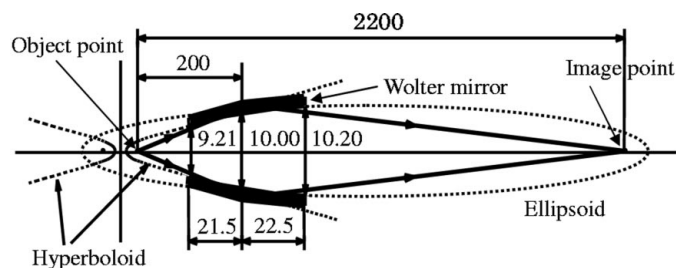


Figure 2
Wolter mirror objective for the X-ray fluorescence microscope. Dimensions in mm.

X-ray fluorescence image was restricted to be about 10 μm because of the figure error of the surface.

3. Performance tests

A specimen that consisted of metallic wires of Cu (diameter 25 μm), Ni (diameter 25 μm), Co (diameter 50 μm) and Fe (diameter 100 μm) was observed in the performance test. Fig. 3(a) shows the X-ray fluorescence image at an excitation X-ray energy of 9.0 keV. This corresponds to the integration image of the X-ray fluorescence. The exposure time was 8 min. To perform the photon counting of the X-ray fluorescence, 240 fluorescence images of 5 s exposure were recorded. To reduce the intensity of the X-ray fluorescence for the photon counting, a sheet of cover glass for an optical microscope was inserted in front of the CCD. The calculated transmittance was 8.0% at 6.4 keV and 28% at 8.04 keV.

When an X-ray photon is absorbed in the depletion region and the induced electrons are within the single pixel, the number of electrons is proportional to the absorbed X-ray energy and this is a single-pixel event. Whereas, when an X-ray photon is absorbed in the pixel

boundary or below the depletion region, the induced electron cloud spreads over the single pixel and this is a multiple-pixel event. To estimate the X-ray energy, it is necessary to extract the single-pixel events. The method of identifying the energy-resolved image is that followed by Tsunemi, Wada *et al.* (1991).

First, the background data were subtracted from the X-ray fluorescence images. The background data recorded without X-ray illumination just before the acquisition of the X-ray fluorescence images were not suitable because the background level was not stable enough. Then, each X-ray fluorescence image smoothed with a rectangular average of 40×40 pixels was regarded as the background data and each smoothed image was subtracted from the original one. The negative-value pixels in the subtracted image were set to be zero.

Second, the single-pixel events were extracted. The event threshold level was set to be 30 in digitized system amplitude units (DN) of the CCD camera system. This level was sufficiently below the X-ray fluorescence energy of Fe. The pixels with values over this were taken as those pixels wherein an X-ray photon was absorbed. The split threshold level was set to be 3 in DN. If the sum of the surrounding eight pixels of the event pixel did not exceed the split threshold level, the event was taken as a single-pixel event. The split threshold level was taken as a slightly large value of the standard deviation of the background data recorded without X-ray illumination, which was 1.64 in DN. Only the single-pixel events were extracted and evaluated.

Third, the pixel values were assigned to the X-ray energy. Fig. 3(b) shows the event histograms extracted from the 240 X-ray fluorescence images. The histograms of Fe, Co, Ni and Cu correspond to the single events from the white rectangle areas in Fig. 3(a). The X-ray energy was calibrated by assigning the peak position of the event histogram of the Cu wire to the energy of Cu $K\alpha$ (8.04 keV). The conversion factor was calculated to be 115 eV per DN. The average energy resolution was 350 eV full width at half-maximum (FWHM). Then, when the pixel value of each single-pixel event was within the FWHM of each element, the pixel was assigned to the corresponding element. Fig. 4 shows the obtained elemental mappings of the specimen. Fig. 4(a) is the integration image and a part of Fig. 3(a). Figs. 4(b), 4(c), 4(d) and 4(e) show the elemental mappings of the Fe, Co, Ni and Cu wires, respectively. Each wire could be imaged separately.

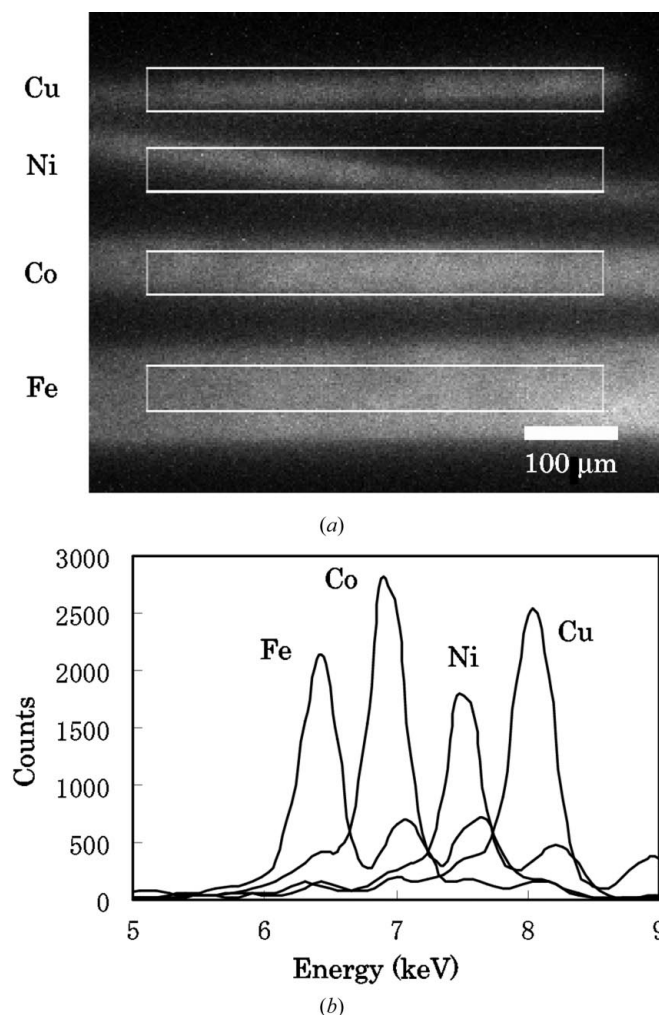


Figure 3
(a) X-ray fluorescence image of metal wires (Cu: diameter 25 μm ; Ni: diameter 25 μm ; Co: diameter 50 μm ; Fe: diameter 100 μm). The exposure time was 8 min. (b) X-ray fluorescence spectra in the white rectangle areas in (a). These spectra were calculated from 240 X-ray fluorescence images recorded on the CCD in the photon-counting condition. The exposure time of each image was 5 s.

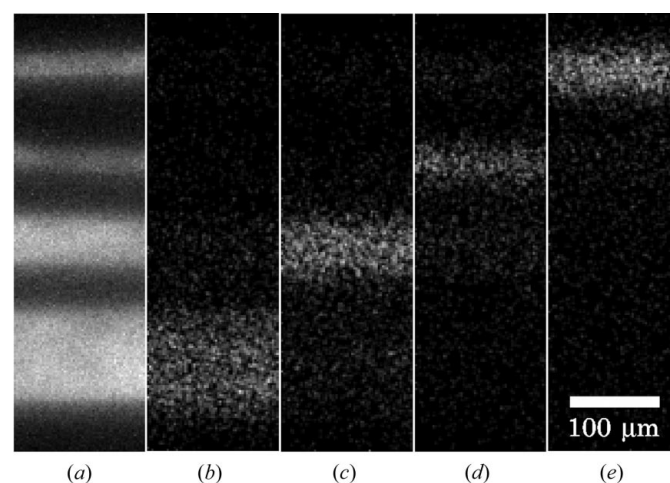


Figure 4
(a) X-ray fluorescence image of metallic wires. Exposure time: 8 min. (b), (c), (d) and (e) Elemental mappings of the metallic wires calculated from 240 photon-counting X-ray fluorescence images. (b) Fe, (c) Co, (d) Ni and (e) Cu.

This method was applied to an elemental analysis of inclusions incorporated in a synthesized diamond. The diamond was synthesized by the solvent method and contained the solvent, such as Fe, Ni and Co, as impurities (Wakatsuki, 1984). Fig. 5(a) is the visible-light image and Fig. 5(b) is the accumulated X-ray fluorescence image. The exposure time was 8 min in the 4×4 pixels binning mode. The excitation X-ray energy was 8.343 keV. To obtain the photon-counting images, 225 images of exposure time 8 s were recorded. The method of identifying the energy-resolved image is the same as previously.

The event histogram was compared with the energy spectrum measured by a Ge SSD (GUL0055, Canberra) at the image plane. The slit width in front of the specimen was set to be 135 μm in the horizontal direction and 30 μm in the vertical direction to illuminate only the upper right inclusion indicated by the white arrow in Fig. 5(b). Fig. 6(a) shows the SSD spectrum of the X-ray fluorescence. The accumulation time was 500 s. Fig. 6(b) shows the event histogram extracted from the corresponding area of the 225 images. The horizontal width could not be determined from the slit width because the optical axis was set normal to the incident X-rays. Then, the horizontal width of the area was set to be the same value as the vertical width of 30 μm . The peaks of the characteristic X-rays of Fe, Co and Ni in the event histogram of Fig. 6(b) are slightly spread out compared with the SSD data in Fig. 6(a). However, these peaks can still be distinguished from each other in Fig. 6(b).

Fig. 7 shows the elemental mappings calculated from these photon-counting images. Fig. 7(a) shows a simply integrated image of the 225 photon-counting images without the extraction of the single events. Figs. 7(b), 7(c) and 7(d) show the elemental mappings of Fe, Co and Ni, respectively. These elemental mappings are blurred compared with Fig. 7(a). This is considered to be due to the statistical noise. The elemental composition ratio of the inclusions in Fig. 7 is almost the same, which is the same result as our previous report (Yamamoto, Watanabe, Takeuchi, Takano, Aota, Kumegawa *et al.*, 2000).

4. Discussion

Tsunemi, Kawai & Hayashida (1991) reported that the energy resolution of the CCD was about 240 eV in FWHM at 5.9 keV. They used a TC-213 CCD (Texas Instruments), which had the same pixel structure as TC-215 which we used. Our result was about 100 eV worse than their result. This is considered to be due to the following reasons.

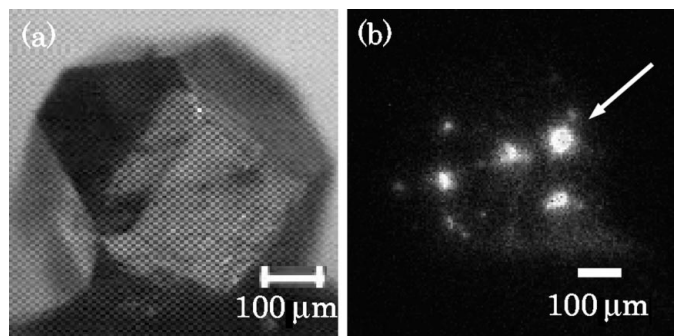


Figure 5
(a) A visible-light image of a synthesized diamond. (b) The corresponding X-ray fluorescence image. The exposure time was 8 min. The white arrow indicates the inclusion from which the X-ray fluorescence was measured by an SSD and a CCD photon-counting system as shown in Fig. 6.

Assuming that the average energy to produce one electron-hole pair in Si is 3.66 eV (Knoll, 2000), a Cu $K\alpha$ X-ray photon (8.04 keV) can induce 2200 electron-hole pairs. This level corresponded to 70 DN in our CCD system. The calculated conversion factor is 31.4 electrons per DN, which corresponds to 115 eV per DN. This relatively large conversion factor may degrade the energy resolution of our system. However, when the amp gain was increased to select the lower conversion factor, the dark noise also increased rapidly. This is due to the large dark noise because the operation temperature was 30 K higher than that of their experiment. X-rays absorbed outside the depletion layer and X-rays absorbed during the readout also increased the image noise. In addition, it is considered that the base level slightly shifted through the background-subtraction process. The average number of events in the white rectangle area of Fe in Fig. 3(a) was 219. There are 16000 pixels in this area. If all the event pixels have a value of 56 DN corresponding to an X-ray energy of 6.4 keV, the average pixel value in this area is calculated to be

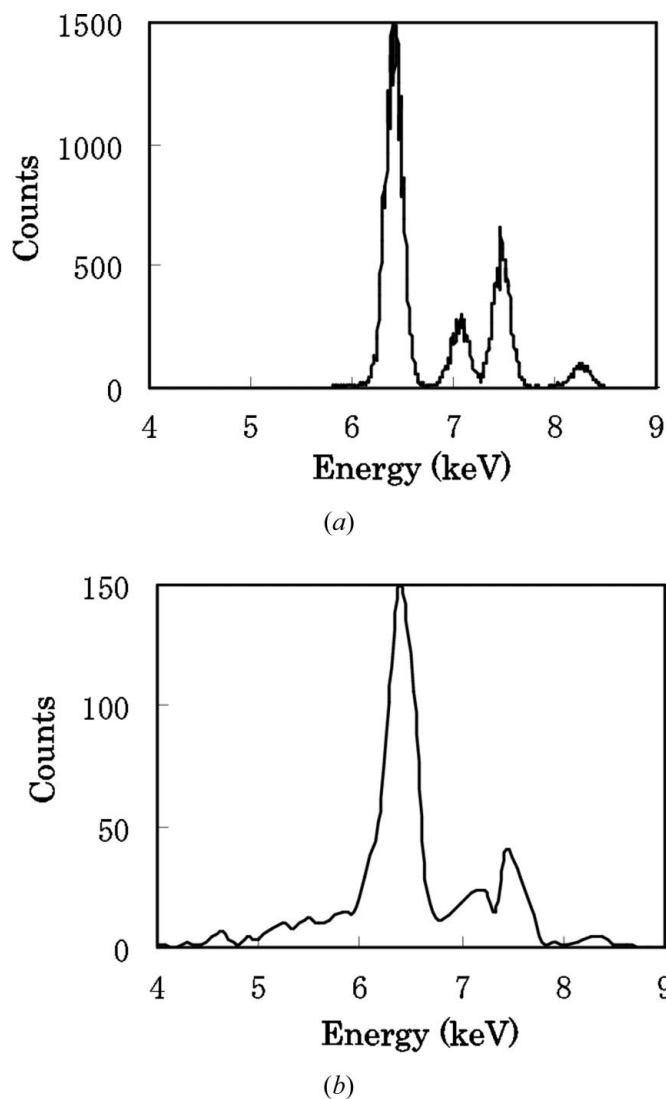


Figure 6
(a) The energy spectrum of X-ray fluorescence from the inclusion of a synthesized diamond indicated in Fig. 5(b) measured by an SSD. The accumulation time was 500 s. (b) The corresponding energy spectrum measured by a CCD photon-counting system. This is calculated from 225 X-ray fluorescence images in the photon-counting condition. The exposure time of each image was 8 s.

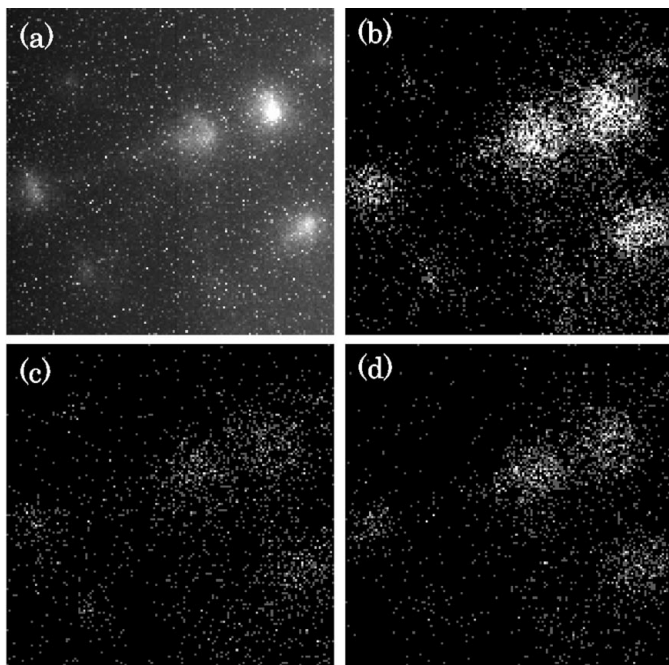


Figure 7

(a) Integrated image of the 225 X-ray fluorescence images of a synthesized diamond in the photon-counting condition. (b), (c) and (d) Elemental mappings of Fe, Co and Ni, respectively.

0.77 DN. In the background-subtraction process, each X-ray fluorescence image smoothed with an area of 40×40 pixels was regarded as the background. Then, the single-event spectrum may slightly shift to the lower energy within 1 DN.

Comparing the energy spectra in Fig. 6(a) with those in Fig. 6(b), the peak intensity of the SSD spectrum in Fig. 6(a) is about one order of magnitude larger than that of the photon counting. Taking into account the exposure times, the SSD intensity is 36 times larger than that of the CCD data. This is due to the low detectable efficiency and the low extraction ratio of the single events. The depth of the depletion layer of the CCD is reported to be about $5 \mu\text{m}$ (Tsunemi, Wada *et al.*, 1991). The detectable efficiency is less than 13% at 6.4 keV, which is calculated by the absorption ratio of the depletion layer. The average extraction ratio of the single-pixel events from all the events was 12% in the case of the synthesized diamond.

In conclusion, two-dimensional elemental maps of the metallic wires, such as Fe, Co, Ni and Cu, and the inclusions of the synthesized

diamond could be obtained with an energy resolution of 350 eV by using the X-ray fluorescence microscope with a Wolter mirror in combination with a CCD photon-counting system. Using this system, not only energy-resolved photon-counting images but also integrated energy flux images by integration of all photon-counting images could be obtained. This system is suitable for an X-ray fluorescence microscope with high resolution and an X-ray microscope with a laboratory X-ray source, because the X-ray intensity must be sufficiently low.

We greatly thank Professor M. Wakatsuki for offering the synthesized diamond and for valuable information on the specimen. This work was partially supported by the Grant-in Aid for Scientific Research (A) No. 11305011 from the Ministry of Education, Culture, Sports, Science and Technology of Japan.

References

- Aoki, S., Takeuchi, A. & Ando, M. (1998). *J. Synchrotron Rad.* **5**, 1117–1118.
- Kagoshima, Y., Ibuki, T., Takai, K., Yokoyama, Y., Miyamoto, N., Tsusaka, Y. & Matsui, J. (2000). *Jpn. J. Appl. Phys.* **39**, L433–L435.
- Knoll, G. F. (2000). *Radiation Detection and Measurement*, p. 357. New York: John Wiley.
- Lengeler, B., Schroer, C. G., Benner, B., Günzler, T. F., Kuhlmann, M., Tümmeler, J., Simionovici, A. S., Drakopoulos, M., Snigirev, A. & Snigireva, I. (2001). *Nucl. Instrum. Methods A*, **467/468**, 944–950.
- SPring-8 (1998). *SPring-8 Annual Report 1998*, pp. 67–68. SPring-8, Hyogo 679-5198, Japan.
- Stern, R. A., Liewer, K. & Janesick, J. R. (1983). *Rev. Sci. Instrum.* **54**, 198–205.
- Strüder, L. (2000). *Nucl. Instrum. Methods A*, **454**, 73–113.
- Takeuchi, A., Aoki, S., Yamamoto, K., Takano, H., Watanabe, N. & Ando, M. (2000). *Rev. Sci. Instrum.* **71**, 1279–1285.
- Tsunemi, H., Kawai, S. & Hayashida, K. (1991). *Jpn. J. Appl. Phys.* **30**, 1299–1302.
- Tsunemi, H., Wada, M., Hayashida, K. & Kwai, S. (1991). *Jpn. J. Appl. Phys.* **30**, 3540–3544.
- Wakatsuki, M. (1984). *Materials Science of the Earth's Interior*, edited by I. Sunagawa, pp. 351–374. Tokyo: Terra Scientific.
- Watanabe, N., Yamamoto, K., Takano, H., Ohigashi, T., Yokosuka, H., Aota, T. & Aoki, S. (2001). *Nucl. Instrum. Methods A*, **467/468**, 837–840.
- Yamamoto, K., Watanabe, N., Takeuchi, A., Takano, H., Aota, T., Fukuda, M. & Aoki, S. (2000). *J. Synchrotron Rad.* **7**, 34–39.
- Yamamoto, K., Watanabe, N., Takeuchi, A., Takano, H., Aota, T., Kumegawa, M., Ohigashi, T., Tanoue, R., Yokosuka, H. & Aoki, S. (2000). *X-ray Microscopy: Proceedings of the Sixth International Conference*, edited by W. Meyer-Ilse, T. Warwick & D. Attwood, pp. 259–262. New York: American Institute of Physics.